



## OPEN ACCESS

## EDITED BY

Mariastefania Antica,  
Rudjer Boskovic Institute, Croatia

## REVIEWED BY

Sourav Mandal,  
University of Liège, Belgium  
Zhengwei Huang,  
Jinan University, China

## \*CORRESPONDENCE

António J. Salgado,  
✉ asalgado@med.uminho.pt  
Bruno F. B. Silva,  
✉ bruno.silva@empa.ch

RECEIVED 07 March 2024

ACCEPTED 03 March 2025

PUBLISHED 21 March 2025

## CITATION

Barata-Antunes S, Sousa RA, Salgado AJ and  
Silva BFB (2025) Whole secretome of  
mesenchymal stem cells is fully incorporated in  
lipid bicontinuous cubic phases.  
*Front. Med. Eng.* 3:1397406.  
doi: 10.3389/fmede.2025.1397406

## COPYRIGHT

© 2025 Barata-Antunes, Sousa, Salgado and  
Silva. This is an open-access article distributed  
under the terms of the [Creative Commons  
Attribution License \(CC BY\)](https://creativecommons.org/licenses/by/4.0/). The use,  
distribution or reproduction in other forums is  
permitted, provided the original author(s) and  
the copyright owner(s) are credited and that the  
original publication in this journal is cited, in  
accordance with accepted academic practice.  
No use, distribution or reproduction is  
permitted which does not comply with these  
terms.

# Whole secretome of mesenchymal stem cells is fully incorporated in lipid bicontinuous cubic phases

Sandra Barata-Antunes<sup>1,2,3,4</sup>, Rui A. Sousa<sup>3</sup>, António J. Salgado<sup>1,2\*</sup>  
and Bruno F. B. Silva<sup>4,5,6,7\*</sup>

<sup>1</sup>Life and Health Sciences Research Institute (ICVS), School of Medicine, University of Minho, Braga, Portugal, <sup>2</sup>ICVS/3B's – PT Government Associated Laboratory, Braga, Portugal, <sup>3</sup>Stemmatters, Biotechnologia e Medicina Regenerativa SA, Guimarães, Portugal, <sup>4</sup>INL – International Iberian Nanotechnology Laboratory, Braga, Portugal, <sup>5</sup>Empa, Swiss Federal Laboratories for Materials Science and Technology, Center for X-ray Analytics, St. Gallen, Switzerland, <sup>6</sup>Empa, Swiss Federal Laboratories for Materials Science and Technology, Laboratory for Biointerfaces, St. Gallen, Switzerland, <sup>7</sup>Empa, Swiss Federal Laboratories for Materials Science and Technology, Laboratory for Biomimetic Membranes and Textiles, St. Gallen, Switzerland

Lipid bicontinuous cubic phases are precursors to cubosomes—a promising type of nanoparticle for the delivery of multicomponent biomolecular mixtures for applications in health such as regenerative medicine and wound healing. In this study, we showed that the secretome of mesenchymal stem cells (MSCs), a complex mixture of growth factors, cytokines, extracellular vesicles, and other cell-secreted molecules with therapeutic potential, can be fully incorporated into the bicontinuous cubic phases of phytantriol and monoolein. When the secretome was added to dry lipid films, the resulting partial phase diagrams of these lipid-secretome systems, although more complex, resemble those of their lipid-water analogs. Remarkably, visual inspections and Small-Angle X-ray Scattering (SAXS) studies showed composition regions of homogeneous solid-like lipid mesophases without excess liquid phase-separation. This indicates that the diverse secretome components, even with their varied sizes and structures, are fully integrated into the cubic phases. SAXS showed patterns dominated by bicontinuous cubic phases with structural parameters close to the lipid-water systems. This suggests that water-soluble proteins likely localize within the water channels of the bicontinuous cubic phase, which must exhibit flexibility to accommodate proteins of diverse sizes, likely through the formation of locally disordered channels. Extracellular vesicles and associated membrane proteins, on the other hand, are likely fusing with and integrating into the cubic membranes. These findings underscore the potential of such liquid crystalline materials as matrices for the entire secretome, paving the way for future secretome-based cell-free therapeutics such as tissue regeneration, neuroprotective and anti-inflammatory treatments.

## KEYWORDS

mesenchymal stem cells, secretome, bicontinuous cubic phases, monoolein, phytantriol, small-angle X-ray scattering (SAXS), extracellular vesicles (EVs), cubosomes

## 1 Introduction

Mesenchymal Stem Cells (MSCs) are multipotent progenitor cells with the capacity to self-renew and proliferate (Friedenstein et al., 1970; Friedenstein et al., 1974). They can be isolated from various sources such as bone marrow, adipose tissue and peripheral blood (Kalervo Väänänen, 2005; Merimi et al., 2021; Wright et al., 2021). MSC-based therapies have been extensively studied for over five decades for regenerative medicine and tissue engineering applications (Fitzsimmons et al., 2018; Zhou et al., 2021). Initially, their therapeutic potential was thought to result from their differentiation capacity. However, increasing evidence now indicates that their paracrine effects, particularly through the secretion of the “secretome,” play a vital role (Gwam et al., 2021; Han et al., 2022). The secretome, a complex set of molecules and biological factors secreted by cells into the extracellular space, includes cytokines, chemokines, growth factors, and extracellular vesicles (EVs) (Brennan et al., 2020). This diverse array has shown promise in modulating the immune system and aiding tissue remodeling in regenerative processes (Gwam et al., 2021; Han et al., 2022).

The significance of the MSC secretome was first highlighted in 2005 by Gneccchi et al., in the context of ischemic heart injury (Gneccchi et al., 2005). Subsequently, several studies have demonstrated the benefits of the MSC-derived secretome across a spectrum of pathological conditions (Han et al., 2022; Múzes and Sipos, 2022; Mendes-Pinheiro et al., 2019; Teixeira et al., 2017). The use of MSC secretome as a cell-free therapeutic alternative also circumvents the challenges associated with cell-based therapies, such as tumorigenicity, immune reactions, and the risk of pathogen transmission (Lo and Parham, 2009; Volarevic et al., 2018). Nonetheless, the diverse nature of the secretome, which includes RNA, proteins, and EVs, combined with their short circulation half-lives (often just minutes), poses a significant challenge in terms of delivery (Werle and Bernkop-Schnürch, 2006; Yang et al., 2003; Akbarian and Chen, 2022).

A search for materials efficient at encapsulating and delivering whole secretome in different clinical contexts is therefore urgent. Currently, most approaches to encapsulate whole secretome are based on naturally derived, synthetic, or chemically modified naturally derived polymers, which are used more broadly as cell and tissue instructive materials (CTIMs). These materials serve primarily as scaffolds or carriers for bioactive compounds, such as proteins and nucleic acids (Rocha et al., 2020; Yang et al., 2003; Ribeiro et al., 2022). The use of CTIMs for delivering the secretome has emerged as a promising strategy in regenerative medicine, particularly to overcome the challenge of low retention rates of bioactive compounds after injection, as well as to provide a controlled release platform for tissue regeneration. Several approaches, including the binding or enclosing of secretome bioactives within a biomaterial matrix, have been explored. These approaches offer multiple advantages: they increase bioavailability, enable sustained and controlled release, and maintain the stability of secretome, all of which could potentially improve therapeutic efficacy (Brennan et al., 2020).

An alternative approach to polymer-based secretome encapsulation and delivery systems could lie in the use of lipid-based delivery systems. These have demonstrated their clinical

efficacy and versatility, most notably in the development of lipid-mRNA-based COVID-19 vaccines (Wang et al., 2021; Schoenmaker et al., 2021) and other medical formulations (Akinc et al., 2019; Kim et al., 2021). With their biocompatibility, bioavailability, and versatile encapsulation capacity, lipid systems offer promising avenues of exploration as CTIMs in therapeutic applications (Gaspar et al., 2020; Angelova et al., 2011; Allen and Cullis, 2013; Zabara et al., 2019; Salentinig, 2019; Paris et al., 2023; Yaghmur and Moghimi, 2023; Wu et al., 2024).

Among the lipid lyotropic crystal (LC) structures, bicontinuous cubic phases like the gyroid  $Q^G$ , the diamond  $Q^D$ , and the primitive  $Q^P$  (of crystallographic space groups  $Ia\bar{3}d$ ,  $Pn\bar{3}m$  and  $Im\bar{3}m$ , respectively) are particularly promising for encapsulating molecules of diverse polarities (Barriga et al., 2019; Angelova et al., 2011; Zabara and Mezzenga, 2014; Palma et al., 2023; Rakotoarisoa et al., 2021; Rakotoarisoa et al., 2022), aligning well with the complex nature of the MSC secretome.  $Q^G$ ,  $Q^D$ , and  $Q^P$  phases are characterized by two intertwined, continuous water channel networks separated by a continuous lipid bilayer. These bilayers are arranged in triply periodic minimal surfaces extending in three dimensions. While in the  $Q^G$  phase the water channels have a threefold connectivity, in the  $Q^D$  the connectivity is fourfold, and in the  $Q^P$  the connectivity is sixfold (Seddon and Templar, 1995; Kulkarni et al., 2011). The compartmentalization inherent to these LCs enables the encapsulation of molecules with different sizes and polarities in the same system: hydrophilic molecules can be located inside the water channels or closer to the lipid polar headgroups, lipophilic molecules can be located within lipid bilayers, and amphiphilic molecules at the interface (Huang and Gui, 2018). Given the broad composition of the MSC secretome, this feature is especially pertinent when designing CTIMs for its whole encapsulation.

Bicontinuous cubic phases have already been shown to be suitable to encapsulate biomolecules of varying sizes and properties, including small water-soluble proteins such as lysozyme (14.4 kDa) (Zabara et al., 2011), larger molecules such as fibrinogen (340 kDa) (Angelova et al., 2003), as well as many membrane proteins (Conn and Drummond, 2013; Lendermann and Winter, 2003; Conn et al., 2010). When modified with cationic lipids, these mesophases can also successfully encapsulate nucleic acids (Bilalov et al., 2009; Kim and Leal, 2015; Philipp et al., 2023). Moreover, bicontinuous cubic phases can be transformed into cubosomes, which are sub-micron particle dispersions of bicontinuous cubic liquid crystalline phases in water (Larsson, 2000; Spicer, 2005; Akhlaghi et al., 2016; Palma et al., 2023). These are typically stabilized with amphiphilic block copolymers such as F127 and exhibit an internal cubic bicontinuous structure, reminiscent of their parent cubic phases. Additionally, cubosomes interact with cell membranes, facilitating membrane fusion (Kim and Leal, 2015; Jabłonowska et al., 2021). Since their introduction by Larsson in 1989 (Larsson, 1989), these particles offer a promising approach for the encapsulation and delivery of therapeutic molecules and are being explored for a variety of innovative therapeutic applications (Conn and Drummond, 2013; Karami and Hamidi, 2016; Barriga et al., 2019; Yaghmur and Mu, 2021; Oliveira et al., 2022; Tien et al., 2020). Like their parent bicontinuous cubic phases, they can encapsulate a diverse array of bioactive molecules, including therapeutic proteins and peptides. These



cultured in Alpha Minimum Essential Medium (AlphaMEM) supplemented with 10% fetal bovine serum (FBS) and 1% Penicillin-Streptomycin (PenStrep). This expansion continued until passage 6 (P6), at which point cells were harvested using trypsin-EDTA and subsequently inoculated into bioreactors. For 3D culture, a vertical wheel bioreactor with magnetic coupling and a working volume capacity of 0.5 L was used (PBS 0.5MAG model, PBS Biotech). Cytodex 3 microcarrier beads were also used as a substrate for cell attachment. Microcarriers were pre-hydrated by adding a solution of phosphate-buffered saline (PBS) without calcium or magnesium ions (w/o  $\text{Ca}^{2+}$  and  $\text{Mg}^{2+}$ ), along with three drops of Tween 80. This mixture was left to hydrate for a minimum of 3 h at room temperature, after which the beads were rinsed three times in PBS w/o  $\text{Ca}^{2+}$  and  $\text{Mg}^{2+}$ . Following hydration, microcarriers were coated with FBS to enhance cell adhesion. This process involved repeated incubation cycles with FBS and washes in PBS, for a total of six cycles. After the final rinse, the beads were resuspended in PBS and sterilized by autoclaving at 120°C and 1.55 kg/cm<sup>2</sup> (23.25 psi) for 30 min. Sterilized beads were then stored at 4°C until use. To inoculate cells into the bioreactor, the previously prepared microcarriers were firstly washed in AlphaMEM containing 10% FBS and 1% PenStrep, and then, incubated with an additional 200 mL of the same medium under sterile conditions. After 1 h of pre-incubation in the single-use bioreactor vessel at 37°C and 21% oxygen with agitation at 25 rpm, hBM-MSCs expanded in 2D culture were detached, counted, and added to the bioreactor at a density of 24,000 cells per milliliter, with an initial total culture volume of 250 mL. This mixture was incubated for 24 h to allow cell attachment to the microcarriers, and an additional 250 mL of medium was added, bringing the final volume to 500 mL, with the agitation rate increased to 52 rpm. Cells were maintained under these conditions for an additional 48 h. After 72 h in the bioreactor, the microcarriers were allowed to settle to the bottom of the Vessel and the culture media was discarded. The vessel was subsequently washed with 100 mL of Neurobasal-A (NB-A) media with 1% Kanamycin (without serum) and 500 mL of the same media was added to the cells that were incubated for 24 h (37°C, 21% O<sub>2</sub>; 52 rpm). 24h later, the conditioned media (hBM-MSCs secretome) was collected and centrifuged at 300g to remove cell debris or any remaining microcarrier, for 5 min at 4°C. Finally, hBM-MSCs secretome was frozen in liquid nitrogen and stored at -80°C until use. NB-A was used as the conditioning medium, as the ultimate goal of our research is to harvest a neuroprotective secretome. This medium, helps produce a secretome enriched with neurotrophic factors that not only sustains MSCs viability but also promotes the secretion of factors beneficial for regenerative medicine applications including neurological conditions such as Parkinson's disease (Teixeira et al., 2016; Teixeira et al., 2017; Mendes-Pinheiro et al., 2019). Moreover, Neurobasal-A is a serum-free medium, reducing the variability in the secretome composition, by the absence of undefined proteins and other molecules that might interfere with analysis or downstream applications.

## 2.2 Determination of protein concentration of hBM-MSCs secretome

Protein concentration of hBM-MSCs secretome was determined using the Microplate Microassay Protocol by

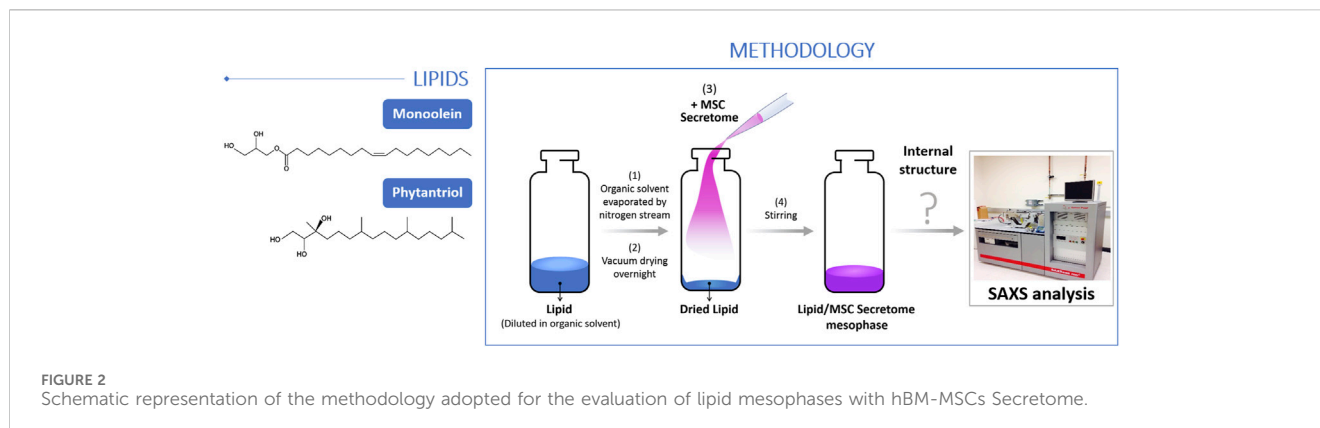
Bradford Assay. For the standard curve, serial dilutions using Bovine Serum Albumin (BSA) protein diluted in NB-A medium (2.5–25 µg/mL) were performed. Subsequently, 150 µL of each standard and hBM-MSCs secretome samples were pipetted to a 96-well plate in triplicate and incubated with 150 µL of Bradford reagent at room temperature. After 10–15 min, the absorbance was read at 595 nm. The blank values were averaged and subtracted from all samples. The concentration of the hBM-MSCs secretome samples was calculated against the standard curve equation.

## 2.3 Characterization of released molecules from hBM-MSC secretome

Two antibody arrays, namely, the Cytokine Antibody Array (RayBio<sup>®</sup> Human Cytokine Antibody Array 5, AAH-CYT-5-4, RayBiotech; [Supplementary Table 1](#)) and RayBio<sup>®</sup> Human Neuroscience Array (RayBio<sup>®</sup> C-Series Human Neuro Discovery Array C1, AAH-NEU-1-4, RayBiotech; [Supplementary Table 2](#)), were used for the identification of cytokines and neurologically relevant proteins in the secretome, respectively, following the kit protocols. Antibody arrays were incubated with secretome under gentle rotation for 24 h at 4°C. Signal intensity of arrays were analyzed by densitometry through chemiluminescence detection, and the relative intensities of individual proteins were calculated after normalizing to the positive controls on each array. Two different hBM-MSC secretome samples (N = 2) were analyzed, with two independent membranes used for each of the antibody array types (cytokine and neuroscience). Data are presented as mean ± SEM for each protein. For proteins identified in both arrays, the values from the cytokine and neuroscience arrays were averaged.

## 2.4 Bulk preparation of lipidic mesophases with hBM-MSC secretome

Phytantriol was purchased from TCI Chemicals (cat. no. P1674, >95% purity) and monoolein from Nu-check prep (cat. no. M-239, >99% purity). Both lipids were used as received, and tested for incorporation of hBM-MSCs secretome ([Figure 2](#)). Briefly, ethanolic solutions of lipid were transferred into 1.5 mL glass vials, after which ethanol was evaporated under vacuum for at least 48 h. This led to the formation of a homogenous lipid film. Subsequently, the hBM-MSCs secretome was added to the dry lipid film according to the intended final lipid/secretome mass ratio. The following mass ratios (w/w) were tested: 70/30, 60/40, 50/50, 40/60 and 30/70 for Monoolein; 85/15, 81/19, 71/29, 70/30, 67/33, 63/37, 60/40, 50/50, 40/60 and 30/70 for Phytantriol. For homogenization, the mixture was left under gentle agitation overnight, followed by centrifugation with the vials in the upside-down and normal positions at 1,500 rpm for 15 min at room temperature. After the centrifugation stage, the samples had a homogenous appearance, and stayed in gentle agitation for two additional days. Finally, the diffraction patterns of the resulting mesophases were obtained by small-angle X-ray scattering (SAXS) to evaluate the structure of the lipid-secretome assemblies.



## 2.5 Small angle X-ray scattering - data collection and analysis

SAXS measurements were performed using a Kratky camera (SAXSess, Anton-Paar, Austria) operating with a slit-geometry, narrowed to ca. 2 mm. The X-ray source (an X-ray copper tube) was operated at 40kV and 50 mA. The emitted radiation is the copper  $k\alpha$  radiation, with a wavelength of 1.5406 Å. The samples were filled in a paste cell between mylar windows and exposed to X-rays for 5–10 min. Scattered X-rays were collected using an image plate. Subsequently, the image plate data was digitalized using an image plate reader, and the 2D data was converted to 1D Intensity vs  $q$  using the SAXS instrument software. To identify the liquid crystalline phases, a homemade Matlab routine was used to analyze the sequence of Bragg reflections.

## 2.6 Statistical analysis

The protein composition of the hBM-MSC Secretome was determined using two different antibody arrays (cytokine and neuroscience arrays, see Section 2.3). For each array type, two different hBM-MSC secretome samples ( $N = 2$ ) were analyzed, with each sample applied to two independent membranes. Given the limited number of samples, our analysis is purely descriptive and data are presented as mean  $\pm$  SEM for each protein based on these duplicate measurements. For proteins detected in both arrays, the values from the cytokine and neuroscience arrays were averaged. Although the small sample size limits statistical significance, our results are in full agreement with extensive analysis from previous work (Pires et al., 2016; Teixeira et al., 2016).

## 3 Results and discussion

### 3.1 Characterization of released molecules from hBM-MSC secretome: Possible therapeutic implications on human diseases

The total protein concentration of hBM-MSCs secretome used in this study was 40  $\mu\text{g}/\text{mL}$ , as determined by Bradford assay. Quantification analysis of protein antibody arrays revealed that the hBM-MSCs secretome is rich in several cell signaling

proteins, crucial for vital functions like apoptosis, angiogenesis, inflammation, immunity, and cell growth and differentiation. These proteins are also implicated in multiple human diseases. The average protein intensities, along with their sizes in kilodaltons (kDa), classes, and Standard Error of the Mean (SEM), are detailed in Supplementary Table 3 and visually represented in Figure 3.

Notably, the secretome exhibited high levels of growth factors (e.g., VEGF, BDNF, FGF-9, IFG-9, IGFBP-2, LIF, NT-3, and TGF- $\beta$ 2) and cytokines (IL-6, IL-8, IL-15), along with chemokines such as MCP-1, MIP-1 $\beta$  (or CCL4), RANTES, TARC, and IP-10. Other proteins, including tissue inhibitor of metalloproteinases (such as TIMP-1) or proteins with osteoclastogenesis inhibitory activity (such as Osteoprotegerin, OPG) were also detected with a substantial amount (Figure 3; Supplementary Table 3). These results are aligned with our previous studies, where proteomic analysis of hBM-MSC-secretome were performed (Pires et al., 2016; Teixeira et al., 2016).

Several of these soluble molecules that were detected in MSC secretome in this study have been extensively reported to be involved in MSC-mediated regeneration and recovery for numerous human diseases affecting different organs and tissues. These diseases include disorders from nervous, cardiovascular, respiratory, skeletal, metabolic, and immune system (Han et al., 2022; Múzes and Sipos, 2022; Mendes-Pinheiro et al., 2019; Teixeira et al., 2017).

### 3.2 Incorporation of hBM-MSCs secretome in bicontinuous cubic phases

In this work, we aimed to investigate the potential of lipid-based bicontinuous cubic phases for encapsulating the entire secretome of Mesenchymal Stem Cells (MSCs). We studied both phytantriol and monoolein lipids, both well-known to form bicontinuous cubic phases (Briggs et al., 1996; Barauskas and Landh, 2003). In water, at room temperature, both lipids form lamellar ( $L_\alpha$ ), gyroid ( $Q^G$ ) and diamond ( $Q^D$ ) bicontinuous cubic phases.

When single proteins are encapsulated in bicontinuous cubic phases, structural changes take place mostly under conditions of restricted hydration (Conn and Drummond, 2013). Typically, bicontinuous cubic phases are found to transition to either inverted hexagonal phases or primitive bicontinuous cubic phases ( $Q^P$ ). In contrast, in the presence of excess water (in

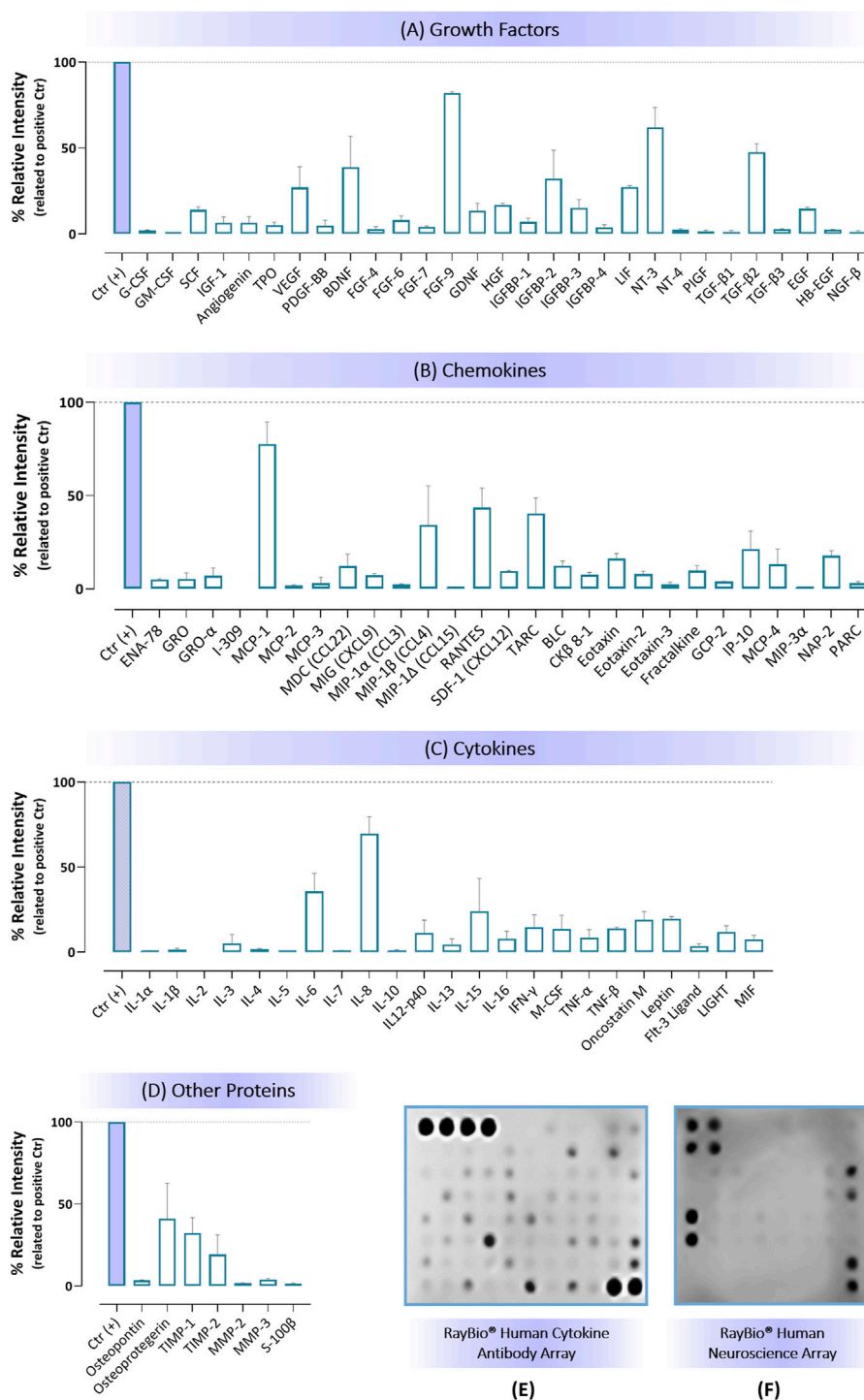


**FIGURE 3** Results regarding protein quantification of hBM-MSC secretome by antibody arrays regarding: (A) Growth factors, (B) Chemokines, (C) Cytokines, and (D) Other proteins, where data are presented as mean of protein relative intensity  $\pm$  SEM. Membrane arrays are shown in (E, F) respectively for: Cytokine Antibody quantification (RayBio® Human Cytokine Antibody Array 5) and Human Neuroscience protein quantification (RayBio® C-Series Human Neuro Discovery Array C1).

the two-phase region), these changes are usually less pronounced. Notably, it has been observed that when encapsulated, water-soluble proteins with sizes larger than the water channels of the cubic phases, lead to no significant changes in the lattice parameters of these phases. This suggests that, despite the

robust evidence of protein encapsulation, the water channels do not expand to fit these larger proteins. Instead, this suggests that such large proteins are accommodated in locally disordered regions, possibly in a sponge-phase-like organization, allowing the organized lattice parameters of the bicontinuous cubic

domains to remain largely unaffected (Angelova et al., 2003; Angelova et al., 2011; Conn and Drummond, 2013).

We will now start by analyzing the phytantriol-secretome system, followed by the monoolein-secretome system. Figures 4A-C show the experimental data obtained from SAXS and visual inspection, and Figure 4D shows an illustration of the different lipid phase structures.

### 3.2.1 The phytantriol-secretome system

The phytantriol-water system has been well-characterized in the literature. At 23°C, the single  $L_{\alpha}$  phase exists between ca. 6 and 14 wt% water, the single  $Q^G$  phase exists between ca. 14 and 24 wt% water, and the single  $Q^D$  phase between ca. 25 and 28 wt% water (Barauskas and Landh, 2003). In between these single-phase regions, exist two-phase regions, and above 28 wt% water, the  $Q^D$  phase coexists with excess water.

When switching from water to MSC secretome, the first important observation is that up to 30 wt% secretome, the whole liquid is incorporated into the lipid phase, which has a soft solid-like appearance characteristic of lipid mesophases. Only in the 33 wt% secretome sample are there signs of a slight excess liquid coexisting with the lipid phase. This simple observation of no excess liquid phase up to 30 wt% secretome indicates that the whole secretome, including all its water-soluble content (e.g., soluble proteins) as well as extracellular vesicles, including their content, are incorporated/encapsulated into the lipid phase. This is remarkable and confirms the potential of lipid-based mesophases to encapsulate a wide array of soluble and membrane proteins. In this case, this capacity is extended to incorporate extracellular vesicles, presumably through fusion of the lipid bilayers of EVs with phytantriol. Another relevant observation is the extension of the lipid-phase region: whereas in the phytantriol-water system the lipid uptakes water until ca. 28 wt% water, after which the  $Q^D$  phase coexists with excess water, in the phytantriol-secretome system, the lipid uptakes the full secretome at least until 30 wt%.

The visual observations provide crucial insights into the capacity of phytantriol to incorporate whole MSC secretome. To obtain structural information about the nature of these phases, we resort to SAXS (Figure 4A).

At 15 wt% secretome, the SAXS pattern shows a single peak. While a single peak by itself makes it difficult to assign to a specific phase, the scattering pattern is most consistent with a lamellar or inverted hexagonal phases, in which the second and higher order reflections are absent. Furthermore, the observed scattering pattern excludes bicontinuous cubic phases. This in contrast with the phytantriol-water system, in which a single gyroid  $Q^G$  phase should be observed between 14 and 24 wt% water. This shows that the inclusion of secretome shifted the gyroid into another structure, most likely a lamellar or hexagonal phase. A transition from a  $Q^G$  phase to a hexagonal phase has been observed in some systems under limited hydration (Conn and Drummond, 2013).

Beyond 15 wt% the system's complexity increases, usually displaying more than one phase. It is important to note that although the samples present a homogeneous appearance, the 2-day equilibration period might not always be sufficient for achieving thermodynamic equilibrium. This period was chosen as a balanced approach to allow sufficient time for homogenization while minimizing the risk of protein degradation. Future studies are

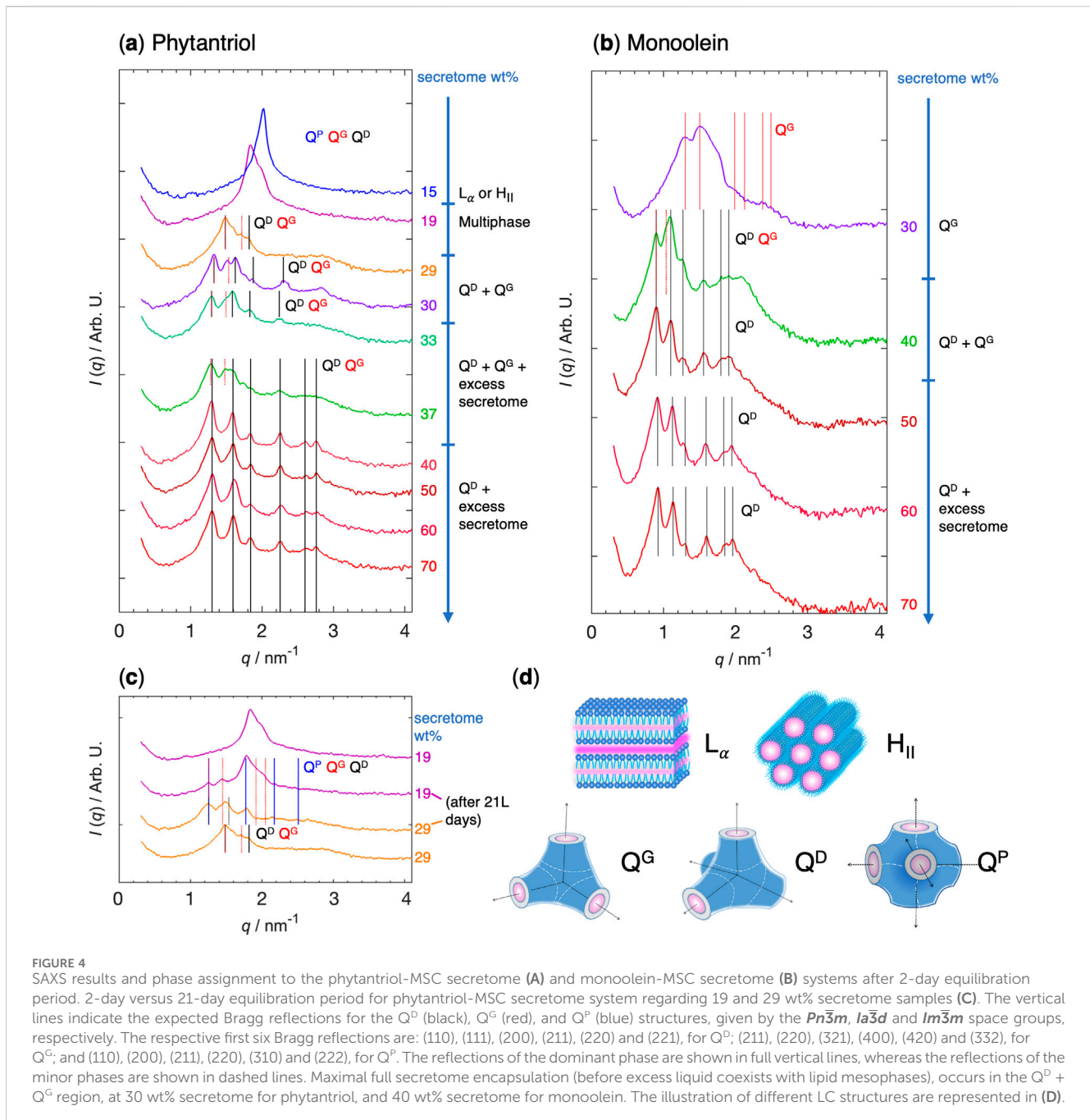
planned to evaluate the stability and functionality of the encapsulated secretome. Nonetheless, the general phase behavior observed for secretome encapsulation within bicontinuous cubic phases is consistent with patterns noted in single-protein encapsulation.

At 19 wt% secretome, the system shows two overlapping peaks, which only by themselves makes the assignment very difficult. Interestingly, when the same sample was measured again 21 days later, the scattering pattern had evolved, with two additional peaks developing at lower  $q$  values, and which make the system now look more consistent with the coexistence between the primitive  $Q^P$  and gyroid  $Q^G$  bicontinuous cubic phases (Figure 4C). While in the phytantriol-water system only a  $Q^G$  single phase should be observed in this composition region, the emergence of a  $Q^P$  is not surprising since these phases have been observed when encapsulating single proteins. This change in scattering patterns observed over time suggests that the initial non-equilibrium state may gradually progress towards equilibrium. Nonetheless, it is important to consider that the initial decision to measure samples after a 2-day equilibration period was made to minimize the risk of protein degradation. Consequently, while longer equilibration times might reveal more about the system's equilibrium state, they also introduce a degree of uncertainty regarding the integrity of the protein components within the system.

When increasing to 29 wt% secretome, the sample shows a scattering pattern somewhat consistent with a coexistence between phases  $Q^D$  and  $Q^G$  (Figure 4A). However, similarly to the 19 wt% case, measuring the samples 21 days later reveals the emergence of additional peaks (Figure 4C). The pattern is now more consistent with a coexistence between the primitive  $Q^P$  and gyroid  $Q^G$  bicontinuous phases, possibly also with the presence of the diamond  $Q^D$ . The peak positions of the  $Q^P$  and  $Q^G$  phases are very close to the positions of the 19 wt% aged sample (note the continuing assignment lines on Figure 4C). Interestingly, all three tentative assignments share the first peak. This existence of three coexisting phases does not violate the Gibbs phase rule, since secretome is a complex mixture, but it is also possible that one of these phases is not in thermodynamic equilibrium.

By increasing the amount of secretome to 30, 33 and 40 wt%, the system is observed to reside within a phase region where both the  $Q^D$  and  $Q^G$  phases coexist. In this region, the SAXS pattern becomes more prominently indicative of the  $Q^D$  phase, facilitating a clearer assignment. The first, third, fourth and fifth peaks of the pattern match the first four reflections of the  $Q^D$  structure. Interestingly, the second peak is consistent with the second reflection of the  $Q^G$  phase, provided that the initial peak corresponds to the first reflection of both  $Q^D$  and  $Q^G$  phases. These samples are therefore likely composed of mostly the  $Q^D$  phase, with small amounts of coexisting  $Q^G$ . As noted above, the 33 and 40 wt% samples already show a slight excess of liquid coexisting with the solid-like lipid mesophases.

The 50, 60 and 70 wt% secretome samples show only the  $Q^D$  pattern, which is now straightforward to assign. The peak positions are also mostly common across the three samples. Since the first signs of excess liquid were observed at 33 wt% secretome, all these three samples are now deep in the two-phase region with large abundance of excess secretome (and water), for



which the sufficient hydration, in line with what is observed in the systems with single proteins, allows the recovery of the  $Q^D$  phase.

The  $d$  spacing of these observed bicontinuous cubic phases is very close to the empty cubic phases (e.g., the lattice spacing at 70 wt% secretome is ca. 6.8 nm, compared to 6.7 nm of phytantriol cubosomes). This behavior, once again, resembles what is found in many single-protein encapsulation systems, and may suggest that the larger proteins might not significantly expand the water channels within the cubic lattices. Instead, these proteins could be inducing locally disordered sponge-like domains within the bicontinuous phases, which are difficult to discern with the used SAXS setup.

### 3.2.2 The monoolein-secretome system

The monoolein-water system has also been thoroughly characterized in the literature. At 25°C, the single  $Q^G$  phase exists between ca. 23 and 37 wt% water, and the single  $Q^D$  phase between ca. 38 and 42 wt% water (Briggs et al., 1996).

When switching to MSC secretome, the monoolein-secretome system shows, in general, similar trends to the phytantriol-secretome system, even though in this case less compositions were studied. The first important observation is that up to 40 wt% secretome, the whole liquid is incorporated into the lipid phase, which has a soft solid-like appearance characteristic of lipid mesophases. Only in the 50 wt% secretome sample are there signs of a slight excess liquid coexisting with the lipid phase. Like

in the phytantriol case, the observation of no liquid phase up to 40 wt% secretome indicates that the whole secretome, including all its water-soluble content (e.g., soluble proteins) as well as extracellular vesicles and their content, are incorporated/encapsulated into the lipid phase. This confirms the potential of lipid-based mesophases to encapsulate not only a wide array of soluble and membrane proteins, but also merging with extracellular vesicles, as it had been already witnessed for the phytantriol system above. Compared to phytantriol, the monoolein has a larger capacity to encapsulate the secretome, which is not entirely surprising, given that it also has a larger swelling in water.

Also here, to obtain structural information about the nature of these phases, we resort to SAXS (Figure 4B). The SAXS pattern for 30 wt% secretome shows the signature of a  $Q^G$  phase, along with a shoulder at  $q = 1.75 \text{ nm}^{-1}$  that we were unable to assign. This  $Q^G$  phase with secretome is well within the expected range for the  $Q^G$  phase in the monoolein-water system.

Increasing the secretome amount to 40 wt% results in a SAXS pattern that is most consistent with the  $Q^D$  phase, with a very good match between the first six peaks and the expected first six reflections of the diamond structure. However, as already witnessed for some compositions in the phytantriol system, there is a shoulder before the second peak that is consistent with the second reflection of the  $Q^G$  phase, provided that the initial peak corresponds to the first reflection of both  $Q^D$  and  $Q^G$  phases. This sample is therefore likely composed of mostly the  $Q^D$  phase, with small amounts of coexisting  $Q^G$ . This behavior is reminiscent of the phytantriol behavior, in which the presence of secretome at limited hydration induced the appearance of traces of the  $Q^G$  phase.

Further increasing the secretome amount to 50 wt% (in the region where macroscopic coexistence with excess liquid is observed) results in SAXS patterns that have an excellent correspondence to a  $Q^D$  phase, without any traces of other lipid mesophases. Interestingly, the peak positions are very close to the peak positions of the  $Q^D$  phase for the 40 wt% secretome sample (Figure 4B). The observation of excess liquid in coexistence with the solid-like lipid phase correlates well with the monoolein-water system, in which the water swelling limit is ca. at 42 wt% water. The remaining two samples, at 60 and 70 wt% secretome show also very similar SAXS patterns, in which the  $Q^D$  phase signature is evident. The peak positions of these phases are also very close to the peak positions of the 40 and 50 wt% secretome samples. In these two-phase regions where  $Q^D$  coexists with excess liquid, the lattice parameter is ca. 9.6 nm, which is slightly smaller than the corresponding value of the monoolein-water system (10.2 nm).

### 3.3 Industrial and clinical aspects

The bicontinuous cubic-secretome phases developed in this study offer significant promise for health applications. In their bulk form, these materials could eventually be directly integrated into wound-healing patches or other topical delivery systems. Moreover, the possibility to transform these phases into cubosomes expands their applicability into diverse delivery modalities (e.g., intravenous injections or intranasal administration). Although sonication is a common method for dispersing bulk cubic phases into cubosomes, its scalability is limited and may damage of sensitive secretome components. Other scalable approaches such as high-pressure homogenization, extrusion or microfluidics may offer interesting alternatives. Importantly, the use of

established lipids like phytantriol and monoolein, which are already used in cosmetic products, anticipates suitable biocompatibility and feasibility of scalable manufacturing for future clinical applications.

## 4 Conclusions and outlook

We have shown that phytantriol- and monoolein-based bicontinuous cubic phases can be used to encapsulate the whole secretome of MSCs, including its diverse composition of proteins and extracellular vesicles. This conclusion stems from the key observation of no excess liquid phase up to 30 wt% secretome for phytantriol and 40 wt% secretome for monoolein, which suggests complete integration of all secretome components within the lipid phase up to these concentrations. The phase behaviors of these lipid-secretome systems, compared to their lipid-water binary system counterparts, show similar trends to those observed in single-protein encapsulation. Particularly, when the secretome uptake is maximized at 30 and 40 wt% for the phytantriol and monoolein systems respectively, before the onset of excess liquid phase separation, the single diamond  $Q^D$  phase characteristic of the lipid-water binary systems gives way to a two-phase coexistence of diamond and gyroid ( $Q^D + Q^G$ ) cubic structures.

Importantly, it is well-established in the literature that  $Q^D$  and  $Q^G$  mesophases, such as those studied here, can be conveniently dispersed into nanosized carriers, known as cubosomes (Larsson, 2000). These cubosomes can be further functionalized to enhance their stability and enable targeted delivery, making them highly promising for a spectrum of therapeutic applications (Barriga et al., 2019). Furthermore, bicontinuous cubic phases have been shown in the past to stabilize individual proteins and retaining their functionality for up to 12 months (Engström et al., 1990). Taken together, these findings on whole-secretome encapsulation by phytantriol and monoolein bicontinuous cubic phases, combined with the potential of cubosome production and functionalization, paves the way for exciting new possibilities in the long-term storage and targeted delivery of the secretome for a variety of secretome-based cell-free therapeutics.

As we look to the future, addressing the bioavailability, stability and functionality of the encapsulated secretome over time will be crucial, along with the development of methods to disperse these materials into cubosomes for therapeutic applications. These efforts are critical to fully realize the potential of these innovative delivery systems in the realm of regenerative medicine and beyond. Our findings open a pathway for further exploration and developments for new therapeutic strategies harnessing the secretome of MSCs.

## Data availability statement

The original contributions presented in the study are included in the article/Supplementary Material, further inquiries can be directed to the corresponding authors.

## Ethics statement

Ethical approval was not required for the studies on humans in accordance with the local legislation and institutional

requirements because only commercially available established cell lines were used.

## Author contributions

SB-A: Conceptualization, Data curation, Formal Analysis, Investigation, Visualization, Writing—original draft. RS: Funding acquisition, Supervision, Writing—review and editing. AS: Funding acquisition, Project administration, Supervision, Writing—review and editing. BS: Formal Analysis, Investigation, Supervision, Validation, Visualization, Writing—review and editing.

## Funding

The author(s) declare that financial support was received for the research and/or publication of this article. This research was funded by Portuguese Foundation for Science and Technology (FCT) through PhD Fellowship attributed to SB-A. (PD/BDE/135568/2018). This work has also been funded by Portuguese National funds, through the FCT - projects UIDB/50026/2020 (DOI 10.54499/UIDB/50026/2020), UIDP/50026/2020 (DOI 10.54499/UIDP/50026/2020) and LA/P/0050/2020 (DOI 10.54499/LA/P/0050/2020); and by the project NORTE-01-0145-FEDER-000039, supported by Norte Portugal Regional Operational Programme (NORTE 2020), under the PORTUGAL 2020 Partnership Agreement, through the European Regional Development Fund (ERDF). This work was also partially supported by “la Caixa” Foundation, (ID 100010434) and Fundação para a Ciência e a Tecnologia, I.P., through Iniciativa Ibérica de Investigación y Innovación Biomedica, under the agreement (LCF/PR/HP20/52300001).

## References

- Akbarian, M., and Chen, S.-H. (2022). Instability challenges and stabilization strategies of pharmaceutical proteins. *Pharmaceutics* 14, 2533. doi:10.3390/pharmaceutics14112533
- Akhlaghi, S. P., Ribeiro, I. R., Boyd, B. J., and Loh, W. (2016). Impact of preparation method and variables on the internal structure, morphology, and presence of liposomes in phytantriol-Pluronic® F127 cubosomes. *Colloids Surfaces B Biointerfaces* 145, 845–853. doi:10.1016/j.colsurfb.2016.05.091
- Akinc, A., Maier, M. A., Manoharan, M., Fitzgerald, K., Jayaraman, M., Barros, S., et al. (2019). The Onpattro story and the clinical translation of nanomedicines containing nucleic acid-based drugs. *Nat. Nanotechnol.* 14, 1084–1087. doi:10.1038/s41565-019-0591-y
- Allen, T. M., and Cullis, P. R. (2013). Liposomal drug delivery systems: from concept to clinical applications. *Adv. drug Deliv. Rev.* 65, 36–48. doi:10.1016/j.addr.2012.09.037
- Angelova, A., Angelov, B., Mutafchieva, R., Lesieur, S., and Couvreur, P. (2011). Self-assembled multicompartiment liquid crystalline lipid carriers for protein, peptide, and nucleic acid drug delivery. *Accounts Chem. Res.* 44, 147–156. doi:10.1021/ar100120v
- Angelova, A., Ollivon, M., Campitelli, A., and Bourgaux, C. (2003). Lipid cubic phases as stable nanochannel network structures for protein biochip development: X-ray diffraction study. *Langmuir* 19, 6928–6935. doi:10.1021/la0345284
- Barauskas, J., and Landh, T. (2003). Phase behavior of the phytantriol/water system. *Langmuir* 19, 9562–9565. doi:10.1021/la0350812
- Barriga, H. M., Holme, M. N., and Stevens, M. M. (2019). Cubosomes: the next generation of smart lipid nanoparticles? *Angew. Chem. Int. Ed.* 58, 2958–2978. doi:10.1002/anie.201804067
- Bilalov, A., Olsson, U., and Lindman, B. (2009). A cubic DNA-lipid complex. *Soft Matter* 5, 3827–3830. doi:10.1039/b908939j
- Brennan, M. Á., Layrolle, P., and Mooney, D. J. (2020). Biomaterials functionalized with MSC secreted extracellular vesicles and soluble factors for tissue regeneration. *Adv. Funct. Mater.* 30, 1909125. doi:10.1002/adfm.201909125
- Briggs, J., Chung, H., and Caffrey, M. (1996). The temperature-composition phase diagram and mesophase structure characterization of the monoolein/water system. *J. de Physique II* 6, 723–751. doi:10.1051/jp2:1996208
- Conn, C. E., Darmanin, C., Sagnella, S. M., Mulet, X., Greaves, T. L., Varghese, J. N., et al. (2010). Incorporation of the dopamine D2L receptor and bacteriorhodopsin within bicontinuous cubic lipid phases. 1. Relevance to in meso crystallization of integral membrane proteins in monoolein systems. *Soft Matter* 6, 4828–4837. doi:10.1039/c0sm00463d
- Conn, C. E., and Drummond, C. J. (2013). Nanostructured bicontinuous cubic lipid self-assembly materials as matrices for protein encapsulation. *Soft Matter* 9, 3449–3464. doi:10.1039/c3sm27743g
- Dos Santos, F., Andrade, P. Z., Boura, J. S., Abecasis, M. M., Da Silva, C. L., and Cabral, J. M. (2010). *Ex vivo* expansion of human mesenchymal stem cells: a more effective cell proliferation kinetics and metabolism under hypoxia. *J. Cell. physiology* 223, 27–35. doi:10.1002/jcp.21987
- Engström, S., Håkanson, H., and Mandenius, C. F. (1990). Enzyme stabilization in composite cubic phases: analytical applications. *Ann. N. Y. Acad. Sci.* 613, 429–430. doi:10.1111/j.1749-6632.1990.tb18193.x
- Fitzsimmons, R. E., Mazurek, M. S., Soos, A., and Simmons, C. A. (2018). Mesenchymal stromal/stem cells in regenerative medicine and tissue engineering. *Stem cells Int.* 2018, 1–16. doi:10.1155/2018/8031718
- Friedenstein, A. J., Chailakhyan, R. K., Latsinik, N. V., Panasyuk, A. F., and Keiliss-Borok, I. V. (1974). Stromal cells responsible for transferring the microenvironment of the hemopoietic tissues: cloning *in vitro* and retransplantation *in vivo*. *Transplantation* 17, 331–340. doi:10.1097/00007890-197404000-00001

## Acknowledgments

We thank the International Iberian Nanotechnology Laboratory for all the collaboration in this work.

## Conflict of interest

Authors SB-A and RS were employed by Stematters, Biotecnologia e Medicina Regenerativa SA.

The remaining author declares that the research was conducted in the absence of any commercial or financial relationships that could be construed as a potential conflict of interest.

The author(s) declared that they were an editorial board member of Frontiers, at the time of submission. This had no impact on the peer review process and the final decision.

## Publisher's note

All claims expressed in this article are solely those of the authors and do not necessarily represent those of their affiliated organizations, or those of the publisher, the editors and the reviewers. Any product that may be evaluated in this article, or claim that may be made by its manufacturer, is not guaranteed or endorsed by the publisher.

## Supplementary material

The Supplementary Material for this article can be found online at: <https://www.frontiersin.org/articles/10.3389/fmede.2025.1397406/full#supplementary-material>

- Friedenstein, A., Chailakhjan, R., and Lalykina, K. (1970). The development of fibroblast colonies in monolayer cultures of Guinea-pig bone marrow and spleen cells. *Cell Prolif.* 3, 393–403. doi:10.1111/j.1365-2184.1970.tb00347.x
- Gaspar, R., Coelho, F., and Silva, B. F. (2020). Lipid-nucleic acid complexes: physicochemical aspects and prospects for cancer treatment. *Molecules* 25, 5006. doi:10.3390/molecules25215006
- Gnecchi, M., He, H., Liang, O. D., Melo, L. G., Morello, F., Mu, H., et al. (2005). Paracrine action accounts for marked protection of ischemic heart by Akt-modified mesenchymal stem cells. *Nat. Med.* 11, 367–368. doi:10.1038/nm0405-367
- Gwam, C., Mohammed, N., and Ma, X. (2021). Stem cell secretome, regeneration, and clinical translation: a narrative review. *Ann. Transl. Med.* 9, 70. doi:10.21037/atm-20-5030
- Han, Y., Yang, J., Fang, J., Zhou, Y., Candi, E., Wang, J., et al. (2022). The secretion profile of mesenchymal stem cells and potential applications in treating human diseases. *Signal Transduct. Target. Ther.* 7, 92–19. doi:10.1038/s41392-022-00932-0
- Huang, Y., and Gui, S. (2018). Factors affecting the structure of lyotropic liquid crystals and the correlation between structure and drug diffusion. *RSC Adv.* 8, 6978–6987. doi:10.1039/c7ra12008g
- Jablonowska, E., Matyszczyk, D., Nazaruk, E., Godlewska, M., Gawel, D., and Bilewicz, R. (2021). Lipid membranes exposed to dispersions of phytantriol and monoolein cubosomes: Langmuir monolayer and HeLa cell membrane studies. *Biochimica Biophysica Acta (BBA) - General Subj.* 1865, 129738. doi:10.1016/j.bbagen.2020.129738
- Kalervo Väänänen, H. (2005). Mesenchymal stem cells. *Ann. Med.* 37, 469–479. doi:10.1080/07853890500371957
- Karami, Z., and Hamidi, M. (2016). Cubosomes: remarkable drug delivery potential. *Drug Discov. today* 21, 789–801. doi:10.1016/j.drudis.2016.01.004
- Kim, H., and Leal, C. (2015). Cuboplexes: topologically active siRNA delivery. *ACS nano* 9, 10214–10226. doi:10.1021/acsnano.5b03902
- Kim, J., Eygeris, Y., Gupta, M., and Sahay, G. (2021). Self-assembled mRNA vaccines. *Adv. drug Deliv. Rev.* 170, 83–112. doi:10.1016/j.addr.2020.12.014
- Kulkarni, C. V., Wachter, W., Iglesias-Salto, G., Engelskirchen, S., and Ahualli, S. (2011). Monoolein: a magic lipid? *Phys. Chem. Chem. Phys.* 13, 3004–3021. doi:10.1039/c0cp01539c
- Larsson, K. (1989). Cubic lipid-water phases: structures and biomembrane aspects. *J. Phys. Chem.* 93, 7304–7314. doi:10.1021/j100358a010
- Larsson, K. (2000). Aqueous dispersions of cubic lipid-water phases. *Curr. Opin. Colloid and Interface Sci.* 5, 64–69. doi:10.1016/s1359-0294(00)00040-6
- Lendermann, J., and Winter, R. (2003). Interaction of cytochrome c with cubic monoolein mesophases at limited hydration conditions: the effects of concentration, temperature and pressure. *Phys. Chem. Chem. Phys.* 5, 1440–1450. doi:10.1039/b209825n
- Lo, B., and Parham, L. (2009). Ethical issues in stem cell research. *Endocr. Rev.* 30, 204–213. doi:10.1210/er.2008-0031
- Mendes-Pinheiro, B., Anjo, S. I., Manadas, B., Da Silva, J. D., Marote, A., Behie, L. A., et al. (2019). Bone marrow mesenchymal stem cells' secretome exerts neuroprotective effects in a Parkinson's disease rat model. *Front. Bioeng. Biotechnol.* 7, 294. doi:10.3389/fbioe.2019.00294
- Merimi, M., EL-Majzoub, R., Lagneaux, L., Moussa Agha, D., Bouhtit, F., Meuleman, N., et al. (2021). The therapeutic potential of mesenchymal stromal cells for regenerative medicine: current knowledge and future understandings. *Front. Cell Dev. Biol.* 9, 661532. doi:10.3389/fcell.2021.661532
- Múzes, G., and Sipos, F. (2022). Mesenchymal stem cell-derived secretome: a potential therapeutic option for autoimmune and immune-mediated inflammatory diseases. *Cells* 11, 2300. doi:10.3390/cells11152300
- Oliveira, C., Ferreira, C. J., Sousa, M., Paris, J. L., Gaspar, R., Silva, B. F., et al. (2022). A versatile nanocarrier—cubosomes, characterization, and applications. *Nanomaterials* 12, 2224. doi:10.3390/nano12132224
- Palma, A. S., Casadei, B. R., Lotierzo, M. C., DE Castro, R. D., and Barbosa, L. R. S. (2023). A short review on the applicability and use of cubosomes as nanocarriers. *Biophys. Rev.* 15, 553–567. doi:10.1007/s12551-023-01089-y
- Paris, J. L., Gaspar, R., Coelho, F., DE Beule, P. A., and Silva, B. F. (2023). Stability criterion for the assembly of core-shell lipid-polymer-nucleic acid nanoparticles. *ACS nano* 17, 17587–17594. doi:10.1021/acsnano.3c07204
- Philipp, J., Dabkowska, A., Reiser, A., Frank, K., Krzysztoń, R., Brummer, C., et al. (2023). pH-dependent structural transitions in cationic ionizable lipid mesophases are critical for lipid nanoparticle function. *Proc. Natl. Acad. Sci. U. S. A.* 120, e2310491120. doi:10.1073/pnas.2310491120
- Pires, A. O., Mendes-Pinheiro, B., Teixeira, F. G., Anjo, S. I., Ribeiro-Samy, S., Gomes, E. D., et al. (2016). Unveiling the differences of secretome of human bone marrow mesenchymal stem cells, adipose tissue-derived stem cells, and human umbilical cord perivascular cells: a proteomic analysis. *Stem cells Dev.* 25, 1073–1083. doi:10.1089/scd.2016.0048
- Rakotoarisoa, M., Angelov, B., Drechsler, M., Nicolas, V., Bizien, T., Gorshkova, Y. E., et al. (2022). Liquid crystalline lipid nanoparticles for combined delivery of curcumin, fish oil and BDNF: *in vitro* neuroprotective potential in a cellular model of tunicamycin-induced endoplasmic reticulum stress. *Smart Mater. Med.* 3, 274–288. doi:10.1016/j.smaim.2022.03.001
- Rakotoarisoa, M., Angelov, B., Espinoza, S., Khakurel, K., Bizien, T., Drechsler, M., et al. (2021). Composition-switchable liquid crystalline nanostructures as green formulations of curcumin and fish oil. *ACS Sustain. Chem. and Eng.* 9, 14821–14835. doi:10.1021/acssuschemeng.1c04706
- Ribeiro, V., Oliveira, J., and Reis, R. (2022). Special issue: tissue engineered biomaterials and drug delivery systems. *Pharmaceutics* 14, 2827. doi:10.3390/pharmaceutics14122827
- Rizwan, S., Assmus, D., Boehnke, A., Hanley, T., Boyd, B., Rades, T., et al. (2011). Preparation of phytantriol cubosomes by solvent precursor dilution for the delivery of protein vaccines. *Eur. J. Pharm. Biopharm.* 79, 15–22. doi:10.1016/j.ejpb.2010.12.034
- Rocha, L. A., Silva, D., Barata-Antunes, S., Cavaleiro, H., Gomes, E. D., Silva, N. A., et al. (2020). Cell and tissue instructive materials for central nervous system repair. *Adv. Funct. Mater.* 30, 1909083. doi:10.1002/adfm.201909083
- Salentinig, S. (2019). Supramolecular structures in lipid digestion and implications for functional food delivery. *Curr. Opin. Colloid and Interface Sci.* 39, 190–201. doi:10.1016/j.cocis.2019.02.002
- Schoenmaker, L., Witzigmann, D., Kulkarni, J. A., Verbeke, R., Kersten, G., Jiskoot, W., et al. (2021). mRNA-lipid nanoparticle COVID-19 vaccines: structure and stability. *Int. J. Pharm.* 601, 120586. doi:10.1016/j.ijpharm.2021.120586
- Seddon, J., and Templer, R. (1995). *Handbook of biological physics*. Elsevier. Polymorphism of lipid-water systems.
- Spicer, P. T. (2005). Progress in liquid crystalline dispersions: cubosomes. *Curr. Opin. Colloid and Interface Sci.* 10, 274–279. doi:10.1016/j.cocis.2005.09.004
- Teixeira, F. G., Carvalho, M. M., Panchalingam, K. M., Rodrigues, A. J., Mendes-Pinheiro, B., Anjo, S., et al. (2017). Impact of the secretome of human mesenchymal stem cells on brain structure and animal behavior in a rat model of Parkinson's disease. *Stem cells Transl. Med.* 6, 634–646. doi:10.5966/sctm.2016-0071
- Teixeira, F. G., Panchalingam, K. M., Assunção-Silva, R., Serra, S. C., Mendes-Pinheiro, B., Patricio, P., et al. (2016). Modulation of the mesenchymal stem cell secretome using computer-controlled bioreactors: impact on neuronal cell proliferation, survival and differentiation. *Sci. Rep.* 6, 27791. doi:10.1038/srep27791
- Tien, N. D., Maurya, A. K., Fortunato, G., Rottmar, M., Zboray, R., Erni, R., et al. (2020). Responsive nanofibers with embedded hierarchical lipid self-assemblies. *Langmuir* 36, 11787–11797. doi:10.1021/acs.langmuir.0c01487
- Volarevic, V., Markovic, B. S., Gazdic, M., Volarevic, A., Jovicic, N., Arsenijevic, N., et al. (2018). Ethical and safety issues of stem cell-based therapy. *Int. J. Med. Sci.* 15, 36–45. doi:10.7150/ijms.21666
- Wang, C., Zhang, Y., and Dong, Y. (2021). Lipid nanoparticle-mRNA formulations for therapeutic applications. *Accounts Chem. Res.* 54, 4283–4293. doi:10.1021/acs.accounts.1c00550
- Werle, M., and Bernkop-Schnürch, A. (2006). Strategies to improve plasma half life time of peptide and protein drugs. *Amino acids* 30, 351–367. doi:10.1007/s00726-005-0289-3
- Wright, A., Arthaud-Day, M. L., and Weiss, M. L. (2021). Therapeutic use of mesenchymal stromal cells: the need for inclusive characterization guidelines to accommodate all tissue sources and species. *Front. Cell Dev. Biol.* 9, 632717. doi:10.3389/fcell.2021.632717
- Wu, Y., Wang, J., Deng, Y., Angelov, B., Fujino, T., Hossain, M. S., et al. (2024). Lipid and transcriptional regulation in a Parkinson's disease mouse model by intranasal vesicular and hexosomal plasmalogen-based nanomedicines. *Adv. Health. Mater.* 13, 2304588. doi:10.1002/adhm.202304588
- Yaghmur, A., and Moghimi, S. M. (2023). Intrinsic and dynamic heterogeneity of nonlamellar lyotropic liquid crystalline nanodispersions. *ACS nano* 17, 22183–22195. doi:10.1021/acsnano.3c09231
- Yaghmur, A., and Mu, H. (2021). Recent advances in drug delivery applications of cubosomes, hexosomes, and solid lipid nanoparticles. *Acta Pharm. Sin. B* 11, 871–885. doi:10.1016/j.apsb.2021.02.013
- Yang, E., VAN Nimwegen, E., Zavolan, M., Rajewsky, N., Schroeder, M., Magnasco, M., et al. (2003). Decay rates of human mRNAs: correlation with functional characteristics and sequence attributes. *Genome Res.* 13, 1863–1872. doi:10.1101/gr.1272403
- Zabara, A., Amar-Yuli, I., and Mezzenga, R. (2011). Tuning in-meso-crystallized lysozyme polymorphism by lyotropic liquid crystal symmetry. *Langmuir* 27, 6418–6425. doi:10.1021/la200710p
- Zabara, A., and Mezzenga, R. (2014). Controlling molecular transport and sustained drug release in lipid-based liquid crystalline mesophases. *J. Control. Release* 188, 31–43. doi:10.1016/j.jconrel.2014.05.052
- Zabara, M., Senturk, B., Gontsarik, M., Ren, Q., Rottmar, M., Maniura-Weber, K., et al. (2019). Multifunctional nano-biointerfaces: cyto-compatible antimicrobial nanocarriers from stabilizer-free cubosomes. *Adv. Funct. Mater.* 29, 1904007. doi:10.1002/adfm.201904007
- Zhou, T., Yuan, Z., Weng, J., Pei, D., DU, X., He, C., et al. (2021). Challenges and advances in clinical applications of mesenchymal stromal cells. *J. Hematol. and Oncol.* 14, 24. doi:10.1186/s13045-021-01037-x